ACS OMEGA

http://pubs.acs.org/journal/acsodf

Article

Coconut Fiber Decorated with Bismuth Vanadate for Enhanced Photocatalytic Activity

Duangdao Channei,* Natthamon Rodsawaeng, Panatda Jannoey, Wilawan Khanitchaidecha, Auppatham Nakaruk, and Sukon Phanichphant

Cite This: *ACS Omega* 2022, 7, 8854−8863

Read Online

ACCESS | Metrics & More | Article Recommendations

ABSTRACT: Bismuth vanadate/coconut fiber ($BiVO_4$/CF) composites were synthesized by coprecipitation and calcination methods. All catalysts used in this work were prepared by a simple coprecipitation method and fully characterized by means of XRD, SEM-EDS, PL, BET N_2 adsorption, zeta potential, and UV−vis DRS. Degradation of indigo carmine (IC) under visible light irradiation was tracked by the UV−vis technique. It was documented that XRD patterns of $BiVO_4$ and $BiVO_4$/CF samples retained the monoclinic structure. From SEM, the CF sheets were visualized, covering the surface of $BiVO_4$ particles. The specific surface area of the synthesized catalysts increased from 1.77 to 24.82 m^2/g. The shift of absorption edge to a longer wavelength corresponded to a decrease in band gap energy from 2.3 to 2.2 eV. The photocatalytic degradation rate of the $BiVO_4$/CF composite was five times higher than that of pristine $BiVO_4$. Moreover, the photocatalyst can be separated and recycled with little change after the third times recycling. The improved activity of the composite resulted from the combination of the adsorption performance of the substrate CF and the photocatalytic activity of $BiVO_4$. In addition, the position of the specific mechanism could occur via both the active species of superoxide radical and hydroxyl radical.

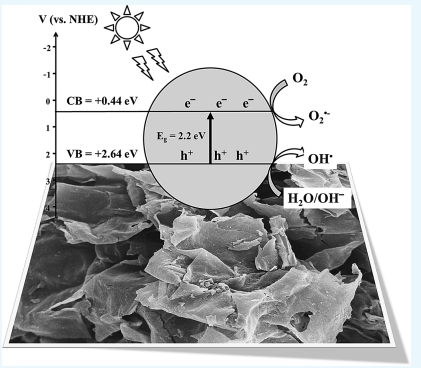

1. INTRODUCTION

The synthetic dye compounds have been used in various manufacturing industries, such as in the textile, plastics, and paper industries. Over 700,000 tons of synthetic dyes is annually produced worldwide.[1] Up to 200,000 tons of textile dye waste from the dyeing process and finishing operations is released to effluents every year.[2] Since the chemical structure of dye molecules is represented by a backbone of the complex aromatic molecular structures that are nonbiodegradable chemicals, they tend to accumulate in an organism and form different aromatic intermediates that are toxic and thus pose a serious threat.[3,4] Furthermore, most of them can persist in the environment and are considered to be the main source of pollution to the environment, which directly affect human health and cause ecological damage even at low concentrations.[5,6]

Various techniques including adsorption, precipitation, crossflow microfiltration, electrodialysis, and reverse osmosis have been used to actively investigate the removal of dye from the environment.[7−11] However, these methods are unproductive at low-concentration contaminants. One of the most promising techniques applied for efficient degradation of antibiotics is advanced oxidation processes (AOPs) based on the use of highly oxidizing species responsible for mineralization of organic pollutants in the presence of a photocatalyst combined with photon energy.[12,13]

The monoclinic phase of bismuth vanadate ($BiVO_4$) with a band gap of 2.4 eV is a semiconductor often used as a heterogeneous photocatalyst for wastewater purification under visible/sunlight irradiation. This material is readily available and possesses various desirable properties, including chemical stability in acidic or alkaline conditions, low toxicity, and strong oxidation properties for water purification.[14−16]

However, some disadvantages in terms of surface properties of the $BiVO_4$ photocatalyst and recombination of photogenerated e^- and h^+ during the process limit its applications in photocatalysis.[17,18] Therefore, the main challenge lies mainly on the design and development by combining the photocatalyst with other materials, which extensively increases the charge transfer and helps separate the e^-/h^+ pair. To prevent charge recombination, heterojunctions with other materials are one example of an effective modification strategy of the photocatalyst for potential applications in photocatalysis.[19−27]

The specific surface area is another important intrinsic property of surface-adsorbed pollutant molecules. Large

Received: December 20, 2021
Accepted: February 18, 2022
Published: March 3, 2022

specific surface areas for the adsorption are an essential step in a photocatalytic reaction because the adsorbed dye molecules from bulk aqueous solution are more likely to react with the photocatalyst and photon energy. Various modification methods have been involved in the modification of the photocatalyst to enhance not only e^-/h^+ recombination but also surface properties.

A heterogeneous photocatalyst in a solid form of the composite with porous carbon-based materials was reported by Xing et al.[28] They prepared the composite material between the TiO_2 photocatalyst and activated carbons from bituminous coal for the degradation of rhodamine B. The nanosized TiO_2 particles on activated carbon could be attributed to the excellent adsorption effect in the dark and high efficiency photocatalytic degradation in the presence of UV light irradiation. They also found that the photocatalytic activity of the composite photocatalyst was dependent on the TiO_2 loading amount.

This result corresponds with the finding of Guo et al.[29] The result was investigated by modifying TiO_2 on powdered activated carbon (TiO_2/PAC) for 2-methylisoborneol (2-MIB) waste treatment. The decolorizations of such a pollutant collected from a river were obtained with adsorption experiments, followed by photodegradation experiments under UV light. The PAC adsorbent does not only enhance the specific surface area of the TiO_2 photocatalyst but also enable the mobility of electrons/holes. Various toxic effluents (like dyes and pesticides) were investigated for the photocatalytic degradation by Sharma et al.[30] It was observed that the mesoporous silica-supported ZnO photocatalyst performed well in absorption capacity.

Another synthetic reactive black KN-B (RB5) dye was investigated for the decolorization by Zhang et al.[31] Immobilizing $BiVO_4$ on activated carbon fibers (ACFs) was reported to be effective in the photocatalytic reaction rather than in single-phase $BiVO_4$. This activity increase was mostly attributed to the formation of interfacial contact between $BiVO_4$ and ACFs, thereby suppressing its charge recombination. The corresponding results were also described by Saleem et al.[32] Their experiments were conducted using monoclinic $BiVO_4$-coated@carbon fibers for the decolorization of synthetic RhB dye under visible light irradiation. $BiVO_4$ with the presence of carbon fibers showed higher photocatalytic activity as compared to pure form. Apart from that, its photocatalytic activity on antimicrobial activity against pathogenic microbes (*Escherichia coli* and *Staphylococcus aureus*) was also investigated. Based on the literature review, the enhanced photocatalytic activity of the photocatalyst combined/supported with highly porous material compared individually with that of the single-phase photocatalyst was mechanically efficient.

Thus, this work contributed to the development of $BiVO_4$ combined with natural coconut fiber (CF). Indigo carmine (IC) dye was used as a degradable substance. IC in bulk was concentrated on the adsorbate surface extracted from CF, while $BiVO_4$ was used as a photoactive phase to degrade the adsorbed IC molecules under visible light. Therefore, carbon material in CF could effectively increase the active surface area and inhibit the recombination of electrons and holes of $BiVO_4$ during photocatalysis.

2. RESULTS AND DISCUSSION

The XRD patterns of CF, pure $BiVO_4$, and the $BiVO_4$/CF composite are provided in Figure 1. The broad peaks of CF

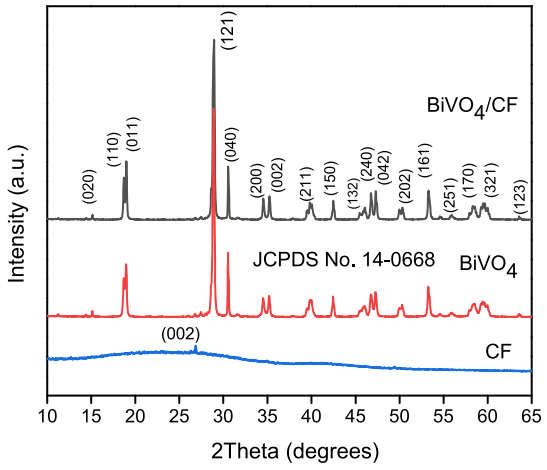

Figure 1. XRD patterns of CF, monoclinic $BiVO_4$ (JCPDS no. 14-0688), and the $BiVO_4$/CF composite.

derived from banana fiber can be indexed to amorphous carbon at $2\theta = 24°$, which correspond to the reflections of the (002) plane. The main peaks can be indexed as (020), (110), (011), (121), (040), (200), (002), (211), (150), (132), (240), (042), (202), (161), (251), (170), (321), and (123) crystal planes of monoclinic $BiVO_4$ (JCPDS no. 14-0668).[33−35] The XRD patterns of the $BiVO_4$/CF composite demonstrate that the existence of CF does not change the crystal structure or form new crystal phases of $BiVO_4$. In addition, no characteristic signal of CF (002) appears in the XRD pattern of the composite sample. This is possibly due to the high crystallinity of the $BiVO_4$ phases, which appear as the dominant peaks in the XRD spectra of the composite sample.

The optical properties of $BiVO_4$ and the $BiVO_4$/CF composite in terms of reflectance spectra (R) were investigated using UV−vis diffuse reflectance spectroscopy (DRS) for solid samples, as shown in Figure 2a. These reflectance data can be converted to the absorption spectra ($F(R)$) according to the Kubelka−Munk (K-M) theory. The K-M equation is given as eq 1.[36]

$$F(R) = \frac{(1 - R)^2}{(2R)} \quad (1)$$

As shown in Figure 2b, the absorption edge of the $BiVO_4$/CF composite exhibited a little shift from 500 to 530 nm, indicating that adding CF in $BiVO_4$ can act as a photosensitizer to effectively improve the visible light response. Tauc plots presented in Figure 2c were used to determine the band gap energy (E_g).[37,38] The band gap values estimated from the intercept of the tangents to the plots are 2.3 and 2.2 eV for $BiVO_4$ and the $BiVO_4$/CF composite, respectively.

Thus, it can be inferred that the band gap of the $BiVO_4$/CF composite became narrower, and the absorption edge was shifted to a longer wavelength by the addition of CF. This can be attributed to the chemically doped and metal ion-implanted semiconductors since the carbon additive derived from coconut fiber could introduce impurity levels within the band gap of $BiVO_4$. This is consistent with the results of Rajamanickam and Shanthi[39] on the TiO_2/activated carbon

https://doi.org/10.1021/acsomega.1c07169
ACS Omega 2022, 7, 8854−8863

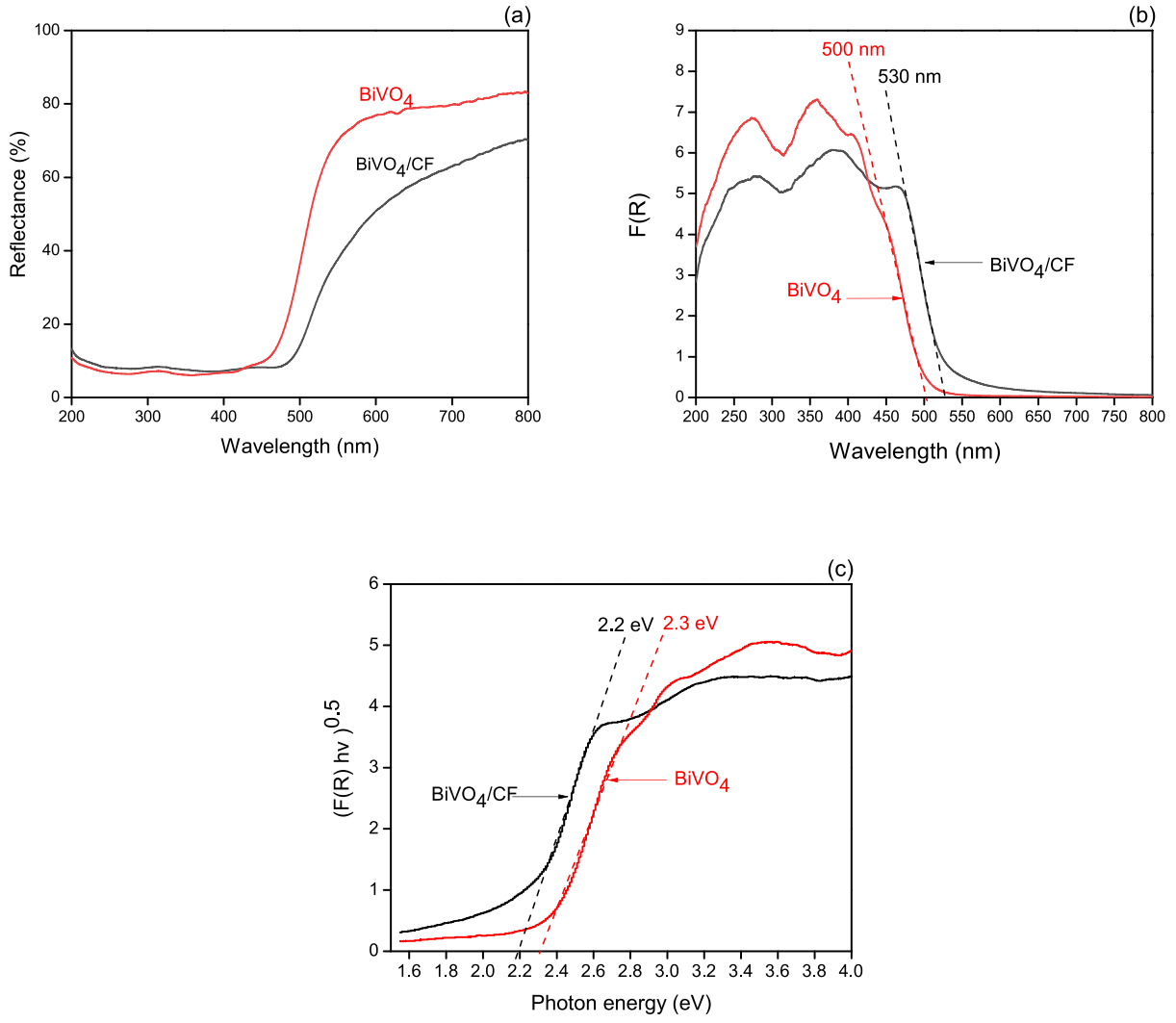

Figure 2. UV−vis DRS of $BiVO_4$ and the $BiVO_4$/CF composite. (a) Diffuse reflectance spectra, (b) absorption spectra, and (c) Tauc plot.

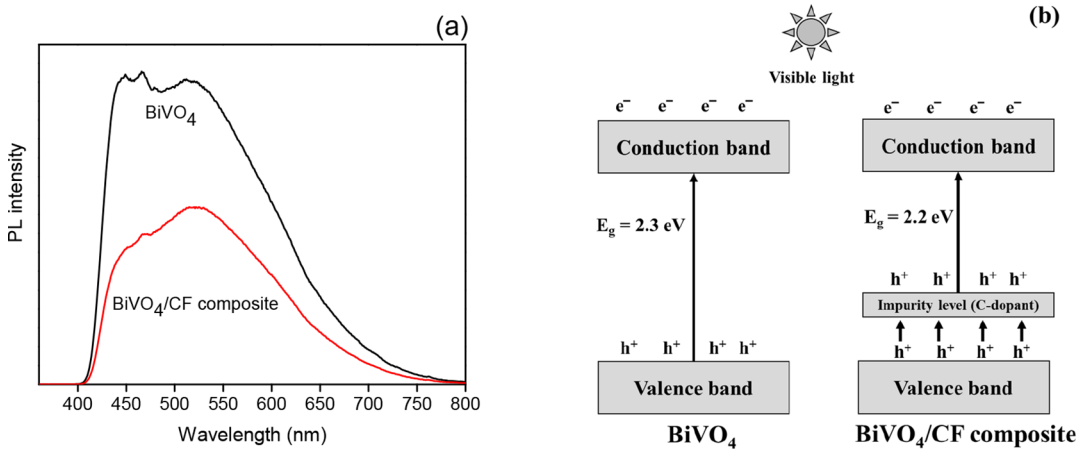

Figure 3. (a) Comparison of the intensity of PL and (b) proposed energy level diagram of $BiVO_4$ and the $BiVO_4$/CF composite.

composite. They found that the composite had a higher absorption edge than the naked TiO_2 in the entire visible region.

Moreover, the photoluminescence (PL) spectra explored the efficiency of separating the photogenerated electron−hole pair of the prepared photocatalysts. Usually, the separation of photogenerated charge carriers is associated with PL signals, in which the lower the PL intensity provided, the higher the separation rate.[40−42] As shown in Figure 3a, the PL emission peak intensity of $BiVO_4$ is higher than that of the $BiVO_4$/CF composite, which is attributed to the decrease in band gap energy in the $BiVO_4$/CF composite according to Figure 3b.

https://doi.org/10.1021/acsomega.1c07169
ACS Omega 2022, 7, 8854−8863

This indicated that the separation and transfer of photogenerated carriers help enhance photocatalytic performance when $BiVO_4$ is modified with CF.

The scanning microscopy images are shown in Figure 4. The SEM images of $BiVO_4$ photocatalysts with different magnifications showed spherical-shaped morphology with the particle size distribution of approximately 6−8 μm. The original CF shows 2D sheet-like morphology with a smooth layer-like surface. After the calcination, the changes in surface morphology of the plate-like structure of CF have been observed. It was covered/mixed with the aggregation of a variety of $BiVO_4$ particles, which increased the probability of adsorbing dye molecules on a high specific surface, resulting in a high photocatalytic activity. Jafry et al.[43] reported similar results after the introduction of silica-decorated P25 TiO_2.

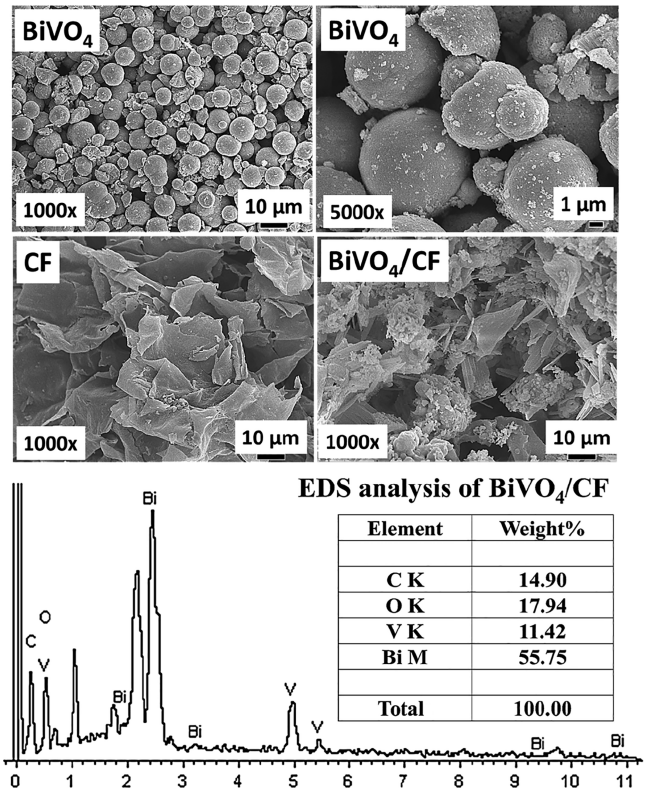

Figure 4. SEM images of the catalysts of $BiVO_4$ and the $BiVO_4$/CF composite and EDS analysis.

In addition, EDS analysis demonstrated further that Bi, O, V, and C coexist in the $BiVO_4$/CF composite as the main elements, which is expected for the composite sample. This further confirmed that the $BiVO_4$/CF composite has been successfully synthesized in this study.

The detailed summary of the specific surface area, pore volume, and average pore size of all samples is presented in Table 1. The $BiVO_4$/CF composite shows a higher surface area (24.82 m^2/g) compared to the pristine $BiVO_4$ (1.77 m^2/g). The increase in the surface area of $BiVO_4$ in the composite is due to the large surface area of CF (391.70 m^2/g) onto the surface of the $BiVO_4$ particles. Besides that, the large surface area and pore volume can enrich the adsorption of organic dyes during photocatalytic activity experiments. This suggested that the photocatalytic and adsorption processes are controlled by not only the external surface of the photocatalyst but also the intraparticle diffusion in the liquid-filled pores. The N_2 adsorption−desorption isotherms of CF, $BiVO_4$, and the $BiVO_4$/CF composite are presented in Figure 5. All samples presented a typical type IV isotherm characteristic with hysteresis loops at the P/P_0 range of 0−1.0, which was related to the characteristics of mesoporous materials (2−50 nm).[44,45] On the other hand, good agreement was also observed for the BJH pore size distribution curve (insets of Figure 5), and the average values of pore size are listed in Table 1. In addition, the quantity adsorbed per gram of composite was found to increase when CF was added, leading to an enhanced specific surface area compared to that in pure $BiVO_4$.

Table 1. Summary Report of the Surface Properties

sample	BET specific surface area (m^2/g)	pore volume (cm^3/g)	pore size (nm)
CF	391.70	0.233	2.79
$BiVO_4$/CF composite	24.82	0.016	3.11
$BiVO_4$	1.77	0.004	5.61

The effect of contact time on IC adsorption on the $BiVO_4$/CF composite was studied for varying adsorption times of 15, 30, 60, and 90 min. The results are illustrated in Figure 6a. It was found that the removal of IC rises rapidly along with the contact time and attains the equilibrium after 30 min. The adsorption study was continued further for 90 min, but no significant increase was observed in IC adsorption. Therefore, 30 min was selected as an equilibrium contact time for dark adsorption before light on in this research.

Figure 6b presents the photodegradations of the IC promoted by photolysis (blank) and photocatalysis with the $BiVO_4$ and $BiVO_4$/CF photocatalysts. The photocatalysis of the pristine $BiVO_4$ curve demonstrates its low efficiency (~16%) for the photodegradation of IC dye, while the photocatalysis of IC reaches ~70% over the $BiVO_4$/CF composite in 120 min. The values of the pseudo-first-order kinetic constants (k) are explained by the pseudo-first-order kinetic model as given in the following equation.[46] The values of the rate constant (k, min^{-1}) were calculated from the slope, as shown in eq 2.

$$-\ln \frac{C_t}{C_0} = kt \tag{2}$$

In these cases, the rate constants were 0.0014 and 0.0082 min^{-1} for $BiVO_4$ and composite material, respectively. This indicated that the photodegradation kinetics of composite material were five times faster than that of the pristine one (Figure 6c).

In general, the increase in activity is due to the greater covering of the surface of the active phase $BiVO_4$ with CF. This would increase the adsorption of dye molecules around the catalyst surface and provide its ability to degrade. Thus, it was noted that the addition of CF in $BiVO_4$ promotes a considerable increase in the IC photodegradation, which serves as another significant way to improve the efficiency of photocatalysts.

Another important factor that affects the degradation rate is the interaction between the catalyst and the dye molecule. The pH of IC aqueous solution also could affect the zeta potential of the photocatalyst. As shown in the inset image (Figure 6b), the point of zero charge (pzc) of $BiVO_4$/CF particles is determined at pH = 11.6. Above the pzc, particles have a

https://doi.org/10.1021/acsomega.1c07169
ACS Omega 2022, 7, 8854−8863

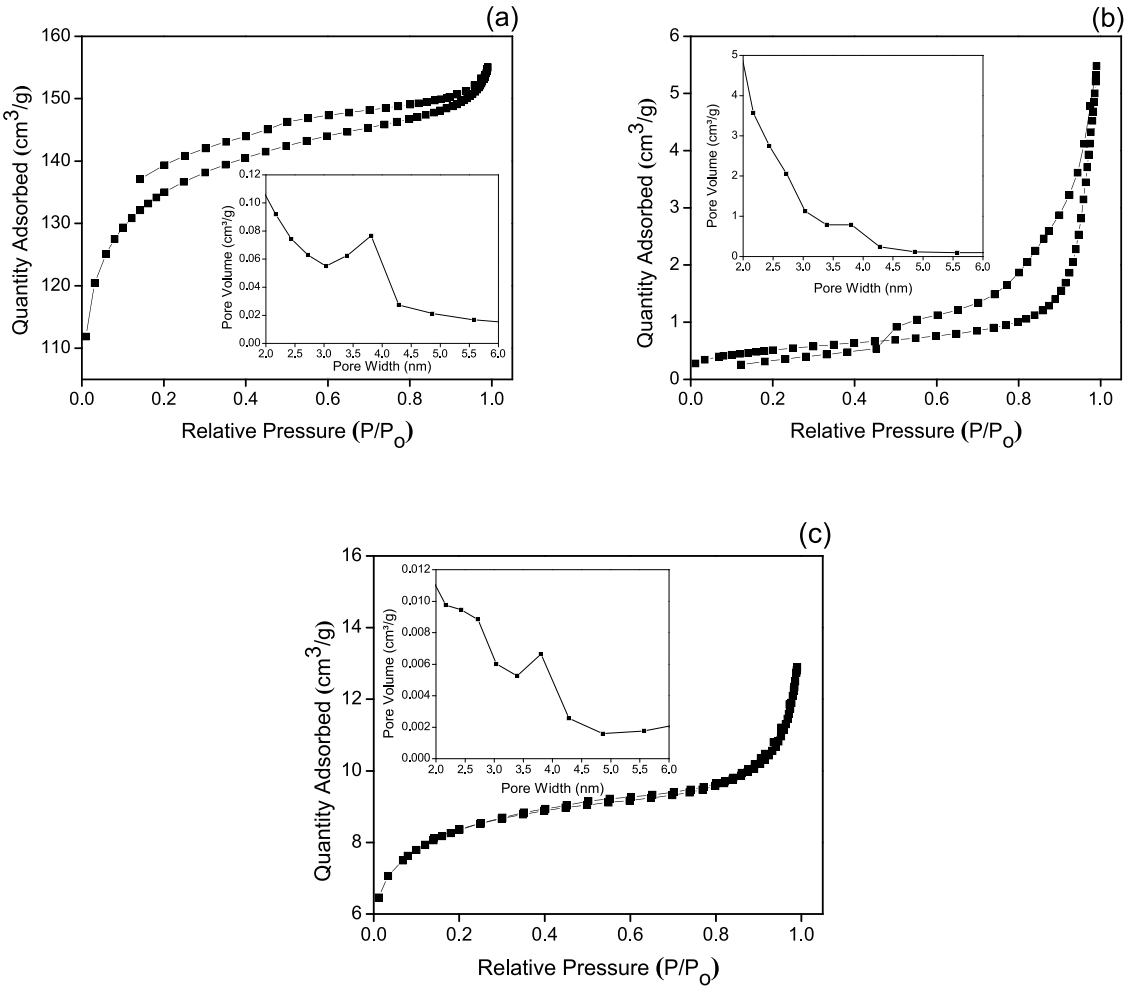

Figure 5. N_2 adsorption−desorption isotherms and pore size distribution (inset): (a) CF, (b) $BiVO_4$, and (c) $BiVO_4$/CF composite.

negative surface charge, whereas the surface is positively charged below this pH. In addition, it was observed that the positive charge of particles presented over a wide range of pH values is due to remaining H^+ residues on the catalyst surface. Since the natural pH of IC is 9, the positive charge is found for $BiVO_4$/CF at this pH. IC dye exists in aqueous solution as negatively charged ions, which favor electrostatic interactions with the positive charge surface of $BiVO_4$/CF particles, leading to the strong adsorption.

To justify the photocatalytic efficiency of $BiVO_4$/CF composites in this study, its potential must be compared with the other activated carbon (AC)-based photocatalysts reported in the literature. Table 2 compares the maximum photocatalytic activities of various pollutants by different activated carbon (AC)-based photocatalysts. In this study, the photocatalysis of IC reached ∼70% over the $BiVO_4$/CF composite in 120 min, whereas if $BiVO_4$ alone was used, ∼16% degradation was achieved, which corresponds well to the reported literature. Based on the results presented in Table 2, the $BiVO_4$/CF composites also exhibited good photocatalytic activity when compared with other similar composite materials.

Furthermore, the photocatalytic stability of the composite was determined by three consecutive experiments under the same reaction condition. Figure 6d compares the results of photocatalytic degradation of IC at the first, second, and third runs. After three consecutive cycles, the degradation efficiency in terms of C_t/C_0 decreased from 70% (1st) to 60% (2nd) and 45% (3rd), which was about 25% compared to the first cycle. This behavior suggested that the catalytic capacity could be mainly affected by the leaching of CF from the composite surface, which decreased the number of active sites for adsorption. Furthermore, the used composite cannot be reused for the fourth cycle due to black CF particles being peeled off from the composite during the process of testing.

To explain the photocatalytic mechanism where photocatalytic reactions happen based on the hydroxyl radical generated via VB or CB, an active species trapping experiment using different scavengers was conducted (see Figure 7a). 5 ppm of *p*-benzoquinone and *t*-butanol was added in the photocatalytic system for superoxide radical anions ($\bullet O_2^-$) and hydroxyl radicals ($HO\bullet$) scavengers, respectively. The results showed that the addition of $O_2^{\bullet-}$ and $HO\bullet$ scavengers inhibited the photocatalytic degradation of IC over the $BiVO_4$/CF composite. It can be concluded that the position of the photocatalytic mechanism could occur via both active species.

In addition, electron spin resonance (ESR) can be used to identify the production of the active oxidation species, as it was described in the literature.[51−53]

The schematic drawing of the proposed energy level of the $BiVO_4$/CF composite is shown in Figure 7b. To find out the conduction band (E_{CB}) and valence band (E_{VB}) edge positions of $BiVO_4$, the values can be calculated following the equations.[54]

https://doi.org/10.1021/acsomega.1c07169
ACS Omega 2022, 7, 8854−8863

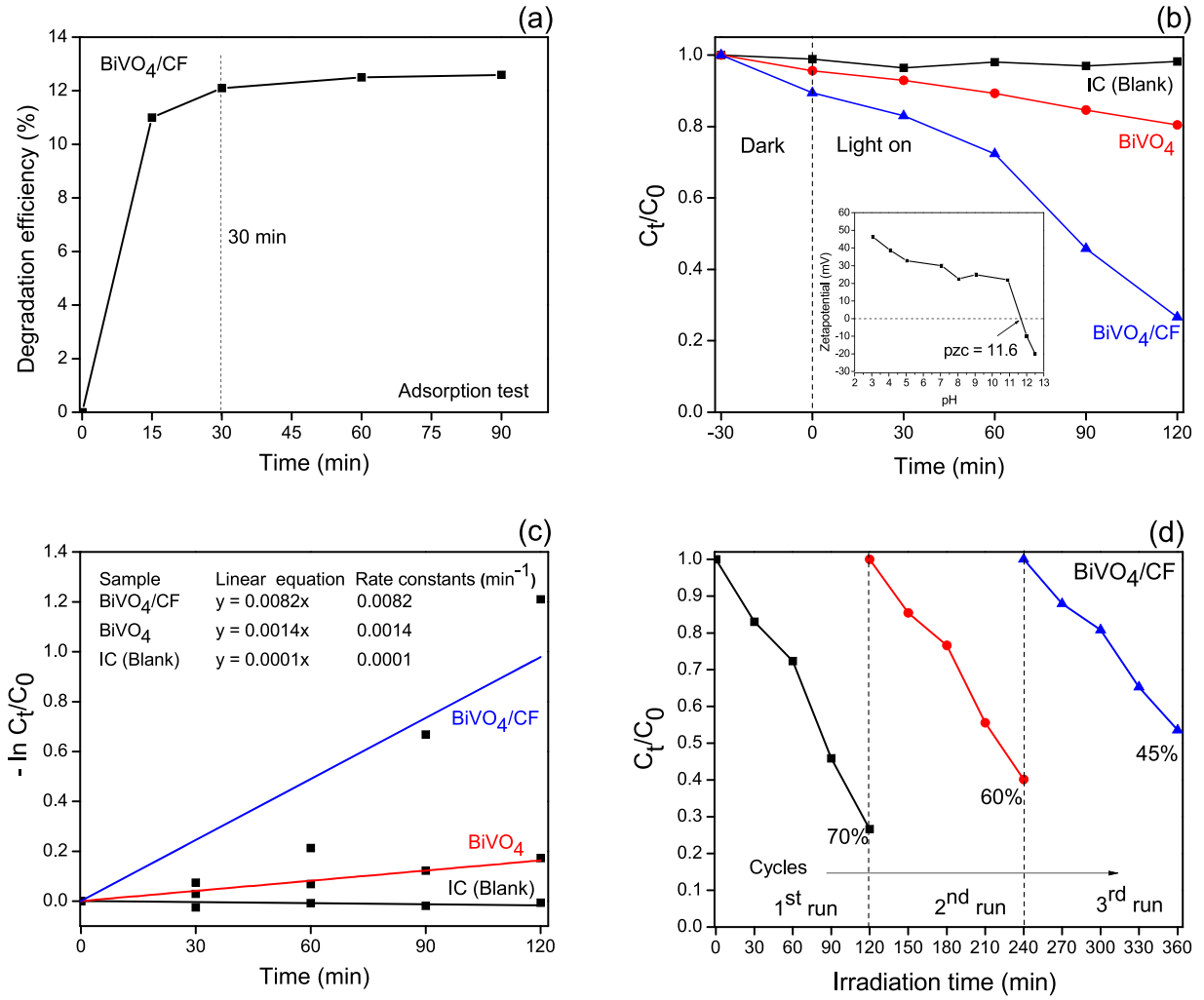

Figure 6. Effect of different photocatalysts on photodegradation of IC: (a) adsorption (b) C_t/C_0, (c) kinetic curves, and (d) reuse of $BiVO_4$/CF.

$$E_{VB} = \chi - E^C + 0.5E_g$$

$$E_{CB} = E_{VB} - E_g$$

The absolute electronegativity (χ) value for $BiVO_4$ equals to 6.04. E^C refers to the energy of the free electron on the hydrogen scale (NHE, 4.5 eV), and E_g is the calculated band gap of the $BiVO_4$/CF composite (2.2 eV). The calculated VB and CB values of $BiVO_4$ in composites are +2.64 and +0.44 eV, respectively.

The general mechanism of the photocatalytic activity of $BiVO_4$ occurs when $BiVO_4$ is illuminated by light such that photon energy equals or exceeds its band gap energy.[55,56] The positive holes (h^+) are produced in the valence band (VB) when the electrons (e^-) from VB are transferred to the conduction band (CB) across the band gap (eq 3). Hydroxyl radicals (HO•) as active species are then generated through the oxidation reaction between the holes with either water (H_2O) or hydroxyl ions (OH^-) as shown in eqs 4 and 5.

$$BiVO_4/CF + \text{photon energy } (h\nu) \rightarrow BiVO_4\ (h^+ + e^-) \quad (3)$$

$$h^+ + H_2O \rightarrow H^+ + HO\bullet \quad (4)$$

$$h^+ + OH^- \rightarrow HO\bullet \quad (5)$$

In the meantime, another strong oxidizing agent such as superoxide radical anions ($\bullet O_2^-$) is also produced at CB by the reaction between e^- and the oxygen molecules (O_2) (eq 6). On the other hand, holes ($\bullet O_2^-$) can subsequently react with H^+ and the produced H_2O_2 molecule in aqueous solution and generate HO• in VB, as shown in eqs 7 and 8.

$$e^- + O_2 \rightarrow \bullet O_2^- \quad (6)$$

$$2(\bullet O_2^-) + 2H^+ \rightarrow O_2 + H_2O_2 \quad (7)$$

$$H_2O_2 + e^- \rightarrow HO\bullet + OH^- \quad (8)$$

These active free radicals (HO•) photo-oxidize the absorbed dye molecules into the degradation products such as CO_2, H_2O, and short-chain fragments.[57] Besides that, CF in the $BiVO_4$ structure can enhance the adsorption of the organic compounds, which facilitates the closeness between photocatalysts and dyes during photocatalysis experiments.

3. CONCLUSIONS

The photocatalysts of $BiVO_4$ supported on coconut fiber (CF) were obtained in situ by the wet chemical process. CF exhibited an important role in the adsorption of IC dyes, while $BiVO_4$ played a more important role in photocatalysis. The XRD diffractograms of the $BiVO_4$/CF composite did not present the signals corresponding with CF. The presence of CF

https://doi.org/10.1021/acsomega.1c07169
ACS Omega 2022, 7, 8854−8863

Table 2. Different AC-Based Photocatalysts Reported in the Literature

photocatalyst	condition	reference
$BiVO_4$ (16%), $BiVO_4$/CF composites (70%)	pollutant: indigo carmine irradiation time: 120 min visible light	present study
TiO_2 (~70%), TiO_2/AC composite (~95.5%)	pollutant: Sunset Yellow irradiation time: 80 min UV light	Rajamanickam and Shanthi[39]
ZnO (k = 0.0051 min^{-1}), ZnO@AC (k = 0.0465 min^{-1})	pollutant: Alizarin cyanine green dye irradiation time: 90 min UV light	Muthirulan et al.[47]
WO_3 (~40%), AC-doped WO_3 (76%)	pollutant: rhodamine B irradiation time: 120 min halide lamp	Tahir et al.[48]
SnO_2 (~9.8%), Co-doped SnO_2 supported on AC (98%)	pollutant: rhodamine B irradiation time: 30 min solar light	Kande et al.[49]
CeO_2 (69%), AC-CeO_2 nanocomposite (94%)	pollutant: methylene blue irradiation time: 60 min sunlight	Jayakumar et al.[50]

material was confirmed by optical, morphological, and surface analysis. After visible light irradiation for 120 min, the $BiVO_4$/CF composite presented faster kinetics than the pristine $BiVO_4$ for IC degradation. There are three possible alternative explanations for the enhanced photocatalytic degradation of IC by the $BiVO_4$/CF composite used in this study: enhanced adsorption characteristics, change in band gap, and/or decreased PL signals, which prolong the recombination life span. The addition of scavengers indicated that both species (hydroxyl radical and superoxide radical) are very reactive toward IC dye degradation. The effective reusability of the $BiVO_4$/CF composite makes it a promising photocatalyst for the degradation of recalcitrant organic pollutants.

4. EXPERIMENTAL SECTION

4.1. Preparation of the Carbonized Adsorbent from Coconut Fiber (CF). Coconut fiber (CF) was collected from Nakhon Sawan Province, Thailand. It was washed thoroughly with tap water to remove dirt on the CF surface and dried at 100 °C for 24 h. Treatment of CF was carried out using acid activation. The process was done by soaking a portion of CF (50 g) in 3 M hydrochloric acid for 24 h. The treated CF was then thermally processed in muffle furnaces at 500 °C for 6 h before storage and use.

4.2. Synthesis of Monoclinic $BiVO_4$. For the experiment, 12 mmol of bismuth nitrate pentahydrate and ammonium vanadate was suspended in 100.0 mL of 2 M nitric acid under mechanical stirring for 30 min. Then, 6 M sodium hydroxide was added dropwise to adjust pH to 5, and then a yellow precipitate was obtained after vigorous stirring for 2 h. Afterward, the solid was removed by centrifugation (8000 rpm, 15 min) and washed several times with deionized water until a neutral pH was reached. The yellow product was further dried in an oven at 70 °C for 24 h. The monoclinic phase of $BiVO_4$ could be obtained after calcination at 500 °C for 4 h.

4.3. Synthesis of the $BiVO_4$/CF Composite. In the case of the $BiVO_4$/CF composite, the as-prepared CF powder (25% w/w) was added to a beaker containing approximately 100.0 L of 6 M H_2SO_4 acid solution with 12 mmol of bismuth nitrate pentahydrate and ammonium vanadate under magnetic stirring for 60 min. The mixed suspension system was further adjusted to pH 5−6 with 6 M sodium hydroxide. After the reaction, the $BiVO_4$/CF composite was separated by centrifugation, washed with DI water, heated at 70 °C for 24 h, and then calcined at 500 °C for 4 h.

4.4. Characterization. Crystallographic structures of the prepared samples were inspected by X-ray diffraction (XRD, Philips X'Pert MPD) with Cu Kα radiation (1.5418 Å). The reflectance of the samples was observed by diffuse reflectance spectroscopy (UV−vis DRS, Agilent 8453 spectrophotometer) from 280 to 800 nm with a 0.2 nm spacing. The photoluminescence (PL) emission spectra were collected on a spectrofluorometer (Horiba Fluoromax-4CP) with an excitation wavelength at 350 nm. Scanning electron micros-

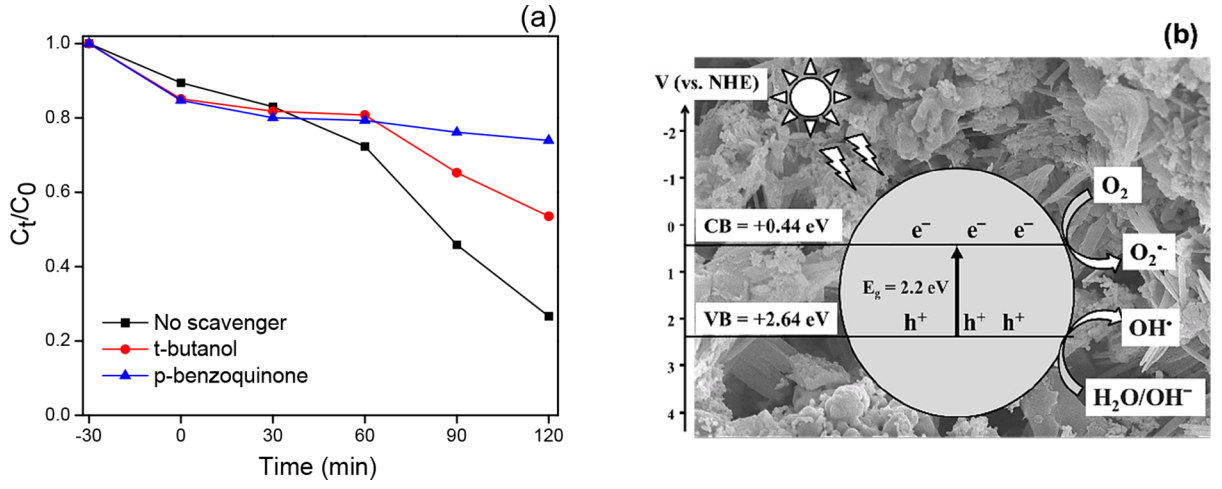

Figure 7. (a) Active species trapping experiment and (b) proposed photocatalysis mechanism of the $BiVO_4$/CF composite for IC degradation.

https://doi.org/10.1021/acsomega.1c07169
ACS Omega 2022, 7, 8854−8863

copy and energy dispersive X-ray spectrometry (SEM/EDS, JSM−6335F, JEOL) were used for morphological feature and elemental analysis. The zeta potential was measured using a zetasizer (Nano ZS4700, Malvern). BET nitrogen adsorption and desorption analysis was applied to measure the specific surface area, pore volume, and pore size distribution based on nitrogen adsorption−desorption isotherms (Micromeritics TriStar II 3020).

4.5. Photocatalytic Activity. For the photocatalytic activity study, the suspensions of 50 mL of 3 M IC aqueous solution were mixed with 0.1 g of photocatalyst. The mixtures were mixed for 30 min without illumination to validate the adsorption−desorption equilibrium of the IC compound throughout the slurry at room temperature.

After that, the photocatalytic degradation of IC was examined under visible light irradiation with a 54 W halogen lamp. The concentration of the IC solution was evaluated and recorded as the initial IC concentration (C_0) to exclude the loss of IC due to the adsorption during mixing in the dark. At given time intervals, 3 mL of suspension was drawn after light irradiation started and each was filtered through centrifugation. The time dependence of the IC concentration (C_t) could be calculated from the calibration curve at a fixed wavelength of 612 nm recorded by a double-beam UV−vis spectrophotometer (Shanghai Mapada Instruments Co., Ltd.).

AUTHOR INFORMATION

Corresponding Author

Duangdao Channei − *Department of Chemistry, Faculty of Science and Centre of Excellence for Innovation and Technology for Water Treatment, Naresuan University, Phitsanulok 65000, Thailand*; orcid.org/0000-0001-8951-3934; Email: duangdaoc@nu.ac.th

Authors

Natthamon Rodsawaeng − *Department of Chemistry, Faculty of Science, Naresuan University, Phitsanulok 65000, Thailand*

Panatda Jannoey − *Department of Biochemistry, Faculty of Medical Science, Naresuan University, Phitsanulok 65000, Thailand*

Wilawan Khanitchaidecha − *Centre of Excellence for Innovation and Technology for Water Treatment and Department of Civil Engineering, Faculty of Engineering, Naresuan University, Phitsanulok 65000, Thailand*

Auppatham Nakaruk − *Centre of Excellence for Innovation and Technology for Water Treatment and Department of Industrial Engineering, Faculty of Engineering, Naresuan University, Phitsanulok 65000, Thailand*; orcid.org/0000-0002-7399-5016

Sukon Phanichphant − *Materials Science Research Center, Faculty of Science, Chiang Mai University, Chiang Mai 50200, Thailand*

Complete contact information is available at: https://pubs.acs.org/10.1021/acsomega.1c07169

Notes

The authors declare no competing financial interest.

ACKNOWLEDGMENTS

This research project is supported by (i) Naresuan University, (ii) Thailand Science Research and Innovation (TSRI), and (iii) National Science, Research and Innovation Fund (NSRF) (grant no. 2324087). The authors also wish to acknowledge the Center of Excellence in Materials Science and Technology, Chiang Mai University, for the chemical materials and other technical assistance under the administration of the Materials Science Research Center, Faculty of Science, Chiang Mai University.

REFERENCES

(1) Berradi, M.; Hsissou, R.; Khudhair, M.; Assouag, M.; Cherkaoui, O.; el Bachiri, A.; El Harfi, A. Textile finishing dyes and their impact on aquatic environs. *Heliyon.* **2019**, *5*, No. e02711.

(2) Xu, X. R.; Li, H. B.; Wang, W. H.; Gu, J. D. Decolorization of dyes and textile wastewater by potassium permanganate. *Chemosphere* **2005**, *59*, 893−898.

(3) Benkhaya, S.; M'rabet, S.; Harfi, A. E. Classifications, properties, recent synthesis and applications of azo dyes. *Heliyon* **2020**, *6*, No. e03271.

(4) Hwang, S. W.; Park, J. H.; Lee, S. L.; Eom, J. H.; Ryu, S. K.; Choi, I. W.; Kim, S. H.; Kang, S. W.; Cho, J. S.; Seo, D. C. Degradation characteristics of non−degradable dye in aqueous solution by ozonation. *Korean J. Environ. Agric.* **2020**, *39*, 58−64.

(5) Lellis, B.; Fávaro-Polonio, C. Z.; Pamphile, J. A.; Polonio, J. C. Effects of textile dyes on health and the environment and bioremediation potential of living organisms. *Biotechnol. Res. Innov.* **2019**, *3*, 275−290.

(6) Bharathiraja, B.; Jayamuthunagai, J.; Praveenkumar, R.; Iyyappan, J. *Phytoremediation techniques for the removal of dye in wastewater, Bioremediation: applications for environmental protection and management*; Springer: Singapore, 2018, 243−252, DOI: 10.1007/978-981-10-7485-1_12.

(7) Wong, S.; Ghafar, N. A.; Ngadi, N.; Razmi, F. A.; Inuwa, I. M.; Mat, R.; Amin, N. A. S. Effective removal of anionic textile dyes using adsorbent synthesized from coffee waste. *Sci. Rep.* **2020**, *10*, 2928.

(8) Zhu, M. X.; Lee, L.; Wang, H. H.; Wang, Z. Removal of an anionic dye by adsorption/precipitation processes using alkaline white mud. *J. Hazard. Mater.* **2007**, *149*, 735−741.

(9) Tolba, G. M. K.; Bastaweesy, A. M.; Ashour, E. A.; Abdelmoez, W.; Khalil, K. A.; Barakat, N. A. M. Effective and highly recyclable ceramic membrane based on amorphous nanosilica for dye removal from the aqueous solutions. *Arab. J. Chem.* **2016**, *9*, 287−296.

(10) Majewska-Nowak, K. M. Treatment of organic dye solutions by electrodialysis. *Membr. Water Treat.* **2013**, *4*, 203−214.

(11) Abid, M. F.; Zablouk, M. A.; Abeer, A. A. Experimental study of dye removal from industrial wastewater by membrane technologies of reverse osmosis and nanofiltration. *Iran. J. Environ. Health Sci. Eng.* **2012**, *9*, 1−9.

(12) Patel, S.; Mondal, S.; Majumder, S. K.; Das, P.; Ghosh, P. Treatment of a pharmaceutical industrial effluent by a hybrid process of advanced oxidation and adsorption. *ACS Omega* **2020**, *5*, 32305−32317.

(13) Cardoso, I. M. F.; Cardoso, R. M. F.; da Silva, J. C. G. E. Advanced oxidation processes coupled with nanomaterials for water treatment. *Nanomaterials* **2021**, *11*, 2045.

(14) Chen, S. H.; Jiang, Y. S.; Lin, H. Easy synthesis of $BiVO_4$ for photocatalytic overall water splitting. *ACS Omega* **2020**, *5*, 8927−8933.

(15) Liu, X.; Gu, S.; Zhao, Y.; Zhou, G.; Li, W. $BiVO_4$, Bi_2WO_6 and Bi_2MoO_6 photocatalysis: A brief review. *J. Mater. Sci. Technol.* **2020**, *56*, 45−68.

(16) Yang, M.; He, H.; Liao, A.; Huang, J.; Tang, Y.; Wang, J.; Ke, G.; Dong, F.; Yang, L.; Bian, L.; Zhou, Y. Boosted water oxidation activity and kinetics on $BiVO_4$ photoanodes with multihigh-index crystal facets. *Inorg. Chem.* **2018**, *57*, 15280−15288.

(17) Abdellaoui, I.; Islam, M. M.; Remeika, M.; Higuchi, Y.; Kawaguchi, T.; Harada, T.; Budich, C.; Maeda, T.; Wada, T.; Ikeda, S.; Sakurai, T. Photocarrier recombination dynamics in $BiVO_4$ for visible light−driven water oxidation. *J. Phys. Chem. C* **2020**, *124*, 3962−3972.

(18) Chen, Z.; Liu, Z.; Zhan, J.; She, Y.; Zhang, P.; Wei, W.; Peng, C.; Li, W.; Tang, J. Resolving the mechanism of oxygen vacancy mediated nonradiative charge recombination in monoclinic bismuth vanadate. *Chem. Phys. Lett.* **2021**, *766*, 138342.
(19) Kong, K.; Fan, H.; Yin, D.; Zhang, D.; Pu, X.; Yao, S.; Su, C. $AgFeO_2$ nanoparticle/znin$_2$s$_4$ microsphere p−n heterojunctions with hierarchical nanostructures for efficient visible-light-driven h2 evolution. *ACS Sustainable Chem. Eng.* **2021**, *9*, 2673−2683.
(20) Shao, Z.; Meng, X.; Lai, H.; Zhang, D.; Pu, X.; Su, C.; Li, H.; Ren, X.; Geng, Y. Coralline-like Ni_2P decorated novel tetrapod-bundle $Cd_{0.9}Zn_{0.1}S$ ZB/WZ homojunctions for highly efficient visible-light photocatalytic hydrogen evolution. *Chin. J. Catal.* **2021**, *42*, 439−449.
(21) Shao, Z.; Zeng, T.; He, Y.; Zhang, D.; Pu, X. A novel magnetically separable $CoFe_2O_4/Cd_{0.9}Zn_{0.1}S$ photocatalyst with remarkably enhanced H_2 evolution activity under visible light irradiation. *Chem. Eng. J.* **2019**, *359*, 485−495.
(22) Jiang, X.; Kong, D.; Luo, B.; Wang, M.; Zhang, D.; Pu, X. Preparation of magnetically retrievable flower-like AgBr/BiOBr/$NiFe_2O_4$ direct Z-scheme heterojunction photocatalyst with enhanced visible-light photoactivity. *Colloids Surf., A* **2022**, *633*, 127880.
(23) He, F.; Meng, A.; Cheng, B.; Ho, W.; Yu, J. Enhanced photocatalytic H_2-production activity of WO_3/TiO_2 step-scheme heterojunction by graphene modification. *Chin. J. Catal.* **2020**, *41*, 9−20.
(24) Wang, K.; Jiang, L.; Wu, X.; Zhang, G. Vacancy mediated z-scheme charge transfer in a 2D/2D $La_2Ti_2O_7$/g-C_3N_4 nanojunction as bifunctional photocatalysts for solar-to-energy conversion. *J. Mater. Chem. A* **2020**, *8*, 13241−13247.
(25) Li, Q.; Zhao, W.; Zhai, Z.; Ren, K.; Wang, T.; Guan, H.; Shi, H. 2D/2D Bi_2MoO_6/g-C_3N_4 S-scheme heterojunction photocatalyst with enhanced visible-light activity by Au loading. *J. Mater. Sci. Technol.* **2020**, *56*, 216−226.
(26) Li, Z.; Wu, Z.; He, R.; Wan, L.; Zhang, S. In_2O_3-x$(OH)_y$/Bi_2MoO_6 S-scheme heterojunction for enhanced photocatalytic performance. *J. Mater. Sci. Technol.* **2020**, *56*, 151−161.
(27) Jiang, T.; Wang, K.; Guo, T.; Wu, X.; Zhang, G. Fabrication of Z-scheme MoO_3/Bi_2O_4 heterojunction photocatalyst with enhanced photocatalytic performance under visible light irradiation. *Chinese J. Catal.* **2020**, *41*, 161−169.
(28) Xing, B.; Shi, C.; Zhang, C.; Yi, G.; Chen, L.; Guo, H.; Huang, G.; Cao, J. Preparation of TiO_2 /activated carbon composites for photocatalytic degradation of RhB under UV light irradiation. *J. Nanomater.* **2016**, *2016*, 1−10.
(29) Guo, X. P.; Zang, P.; Li, Y. M.; Bi, D. S. TiO_2−powdered activated carbon (TiO_2/PAC) for removal and photocatalytic properties of 2−methylisoborneol (2−MIB) in water. *Water* **2021**, *13*, 1622.
(30) Sharma, M.; Hazra, S.; Basu, S. Kinetic and isotherm studies on adsorption of toxic pollutants using porous ZnO@SiO_2 monolith. *J. Colloid Interface Sci.* **2017**, *504*, 669−679.
(31) Zhang, C.; Han, P.; Lu, X.; Mao, Q.; Qu, J.; Li, Y. Preparation and photocatalytic activity characterization of activated carbon fiber−$BiVO_4$ composites. *RSC Adv.* **2018**, *8*, 24665−24672.
(32) Saleem, A.; Ahmed, T.; Ammar, M.; Zhang, H. L.; Xu, H. B.; Tabassum, R. Direct growth of m−$BiVO_4$@carbon fibers for highly efficient and recyclable photocatalytic and antibacterial applications. *J. Photochem. Photobiol.* **2020**, *213*, 112070.
(33) Shang, H.; Lu, Y.; Zhao, F.; Chao, C.; Zhang, B.; Zhang, H. Preparing high surface area porous carbon from biomass by carbonization in a molten salt medium. *RSC Adv.* **2015**, *5*, 75728−75734.
(34) Packiaraj, R.; Devendran, P.; Asath Bahadur, S.; Nallamuthu, N. Structural and electrochemical studies of Scheelite type $BiVO_4$ nanoparticles: synthesis by simple hydrothermal method. *J. Mater. Sci. Mater. Med.* **2018**, *29*, 13265−13276.
(35) Xiong, S.; Wu, T.; Fan, Z.; Zhao, D.; Du, M.; Xu, X. Preparation of a leaf−like $BiVO_4$−reduced graphene oxide composite and its photocatalytic activity. *J. Nanomater.* **2017**, *2017*, 1−12.
(36) Gesesse, G. D.; Gomis-Berenguer, A.; Barthe, M. F.; Ania, C. O. On the analysis of diffuse reflectance measurements to estimate the optical properties of amorphous porous carbons and semiconductor/carbon catalysts. *J. Photochem. Photobiol., A* **2020**, *398*, 112622.
(37) Makuła, P.; Pacia, M.; Macyk, W. How to correctly determine the band gap energy of modified semiconductor photocatalysts based on uv−vis spectra. *J. Phys. Chem. Lett.* **2018**, *9*, 6814−6817.
(38) López, R.; Gómez, R. Band-gap energy estimation from diffuse reflectance measurements on sol−gel and commercial TiO_2: A comparative study. *J. Sol-Gel Sci. Technol.* **2012**, *61*, 1−7.
(39) Rajamanickam, D.; Shanthi, M. Photocatalytic degradation of an azo dye Sunset Yellow under UV-A light using TiO_2/CAC composite catalysts. *Spectrochim. Acta A Mol. Biomol. Spectrosc.* **2014**, *128*, 100−108.
(40) Brüninghoff, R.; Wenderich, K.; Korterik, J. P.; Mei, B. T.; Mul, G.; Huijser, A. Time−dependent photoluminescence of nano-structured anatase TiO_2 and the role of bulk and surface processes. *J. Phys. Chem. C* **2019**, *123*, 26653−26661.
(41) Khan, M. M.; Ansari, S. A.; Pradhan, D.; Ansari, M. O.; Han, D. H.; Lee, J.; Cho, M. H. Band gap engineered TiO_2 nanoparticles for visible light induced photoelectrochemical and photocatalytic studies. *J. Mater. Chem. A* **2014**, *2*, 637−644.
(42) Channei, D.; Nakaruk, A.; Khanitchaidecha, W.; Jannoey, P.; Phanichphant, S. Adsorption and photocatalytic processes of mesoporous SiO_2−Coated monoclinic $BiVO_4$. *Front. Chem.* **2018**, *6*, 1−7.
(43) Jafry, H. R.; Liga, M. V.; Li, Q.; Barron, A. R. Simple route to enhanced photocatalytic activity of P25 Titanium dioxide nanoparticles by silica addition. *Environ. Sci. Technol.* **2011**, *45*, 1563−1568.
(44) Jia, P.; Tan, H.; Liu, K.; Gao, W. Removal of methylene blue from aqueous solution by bone char. *Appl. Sci.* **2018**, *8*, 1903.
(45) Mansour, S.; Akkari, R.; Ben Chaabene, S.; Zina, M. S. Effect of surface site defects on photocatalytic properties of $BiVO_4/TiO_2$ heterojunction for enhanced methylene blue degradation. *Adv. Mater. Sci. Eng.* **2020**, *2020*, 1−16.
(46) Jawad, A. H.; Mubarak, N. S. A.; Ishak, M. A. M.; Ismail, K.; Nawawi, W. I. Kinetics of photocatalytic decolourization of cationic dye using porous TiO_2 film. *J. Taibah Univ. Sci.* **2016**, *10*, 352−362.
(47) Muthirulan, P.; Meenakshisundararam, M.; Kannan, N. Beneficial role of ZnO photocatalyst supported with porous activated carbon for the mineralization of alizarin cyanin green dye in aqueous solution. *Journal of Advanced Research.* **2013**, *4*, 479−484.
(48) Tahir, M. B.; Ashraf, M.; Rafique, M.; Ijaz, M.; Firman, S.; Mubeen, I. Activated carbon doped WO_3 for photocatalytic degradation of rhodamine-B. *Appl. Nanosci.* **2020**, *10*, 869−877.
(49) Kande, S. R.; Zaware, B. H.; Muley, G. G.; Gambhire, A. B. Co-doped SnO_2 supported on activated carbon: an efficient solar photocatalyst for the degradation of rhodamine b. *Asian J. Chem.* **2020**, *32*, 519−527.
(50) Jayakumar, G.; Irudayaraj, A. A.; Raj, A. D. Investigation on the synthesis and photocatalytic activity of activated carbon−cerium oxide (AC−CeO_2) nanocomposite. *Appl. Phys. A: Mater. Sci. Process.* **2019**, *125*, 742.
(51) Wang, H.; Li, X.; Zhao, X.; Li, C.; Song, X.; Zhang, P.; Huo, P.; Li, X. A review on heterogeneous photocatalysis for environmental remediation: From semiconductors to modification strategies. *Chin. J. Catal.* **2022**, *43*, 178−214.
(52) Kougias, P. G.; Angelidaki, I. Biogas and its opportunities—A review. Front. *Environ. Sci. Eng.* **2018**, *12*, 14.
(53) Liu, L.; Hu, T.; Dai, K.; Zhang, J.; Liang, C. A novel step-scheme $BiVO_4/Ag_3VO_4$ photocatalyst for enhanced photocatalytic degradation activity under visible light irradiation. *Chin. J. Catal.* **2021**, *42*, 46−55.
(54) Shao, Q.; Lin, H.; Shao, M. Determining locations of conduction bands and valence bands of semiconductor nanoparticles based on their band gaps. *ACS Omega* **2020**, *5*, 10297−10300.

https://doi.org/10.1021/acsomega.1c07169
ACS Omega 2022, 7, 8854−8863

(55) Li, Z.; Anthony, I.; Xiangchao, M.; Zisheng, Z. Photocatalytic oxidation of methanol to formaldehyde on bismuth−based semiconductors. *J. Hazard. Mater.* **2019**, *380*, 120822.
(56) Chen, Y.; Ma, X.; Li, D.; Wang, H.; Huang, C. Mechanism of enhancing visible−light photocatalytic activity of $BiVO_4$ via hybridization of graphene based on a first−principles study. *RSC Adv.* **2017**, *7*, 4395−4401.
(57) Thongam, D. D.; Chaturvedi, H. Advances in nanomaterials for heterogeneous photocatalysis. *Nano. Express.* **2021**, *2*, No. 012005.

https://doi.org/10.1021/acsomega.1c07169
ACS Omega 2022, 7, 8854−8863